Nanoscale Res Lett (2010) 5:991–1001
DOI 10.1007/s11671-010-9590-5

NANO EXPRESS

# Cooperative Effects in the Photoluminescence of (In,Ga)As/GaAs Quantum Dot Chain Structures

**Yu. I. Mazur · V. G. Dorogan · E. Marega Jr · D. F. Cesar · V. Lopez-Richard · G. E. Marques · Z. Ya. Zhuchenko · G. G. Tarasov · G. J. Salamo**

Received: 20 January 2010 / Accepted: 27 March 2010 / Published online: 16 April 2010


**Abstract** Multilayer $In_{0.4}Ga_{0.6}As/GaAs$ quantum dot (QD) chain samples are investigated by means of cw and time-resolved photoluminescence (PL) spectroscopy in order to study the peculiarities of interdot coupling in such nanostructures. The temperature dependence of the PL has revealed details of the confinement. Non-thermal carrier distribution through in-chain, interdot wave function coupling is found. The peculiar dependences of the PL decay time on the excitation and detection energies are ascribed to the electronic interdot coupling and the long-range coupling through the radiation field. It is shown that the dependence of the PL decay time on the excitation wavelength is a result of the superradiance effect.

**Keywords** Time-resolved photoluminescence · Quantum dot chain · Interdot coupling

E. Marega Jr: On leave from Departamento de Física e Ciência dos Materiais, Instituto de Física de São Carlos-USP São Carlos SP 13560-970, Brazil.

Yu. I. Mazur (✉) · V. G. Dorogan · E. Marega Jr · G. J. Salamo
Department of Physics, University of Arkansas,
226 Physics Building, Fayetteville, AR 72701, USA
e-mail: ymazur@uark.edu

D. F. Cesar · V. Lopez-Richard · G. E. Marques
Departamento de Fisica, Universidade Federal de Sao Carlos,
13565-905 Sao Carlos, Sao Paulo, Brazil

Z. Ya. Zhuchenko · G. G. Tarasov
Institute of Semiconductor Physics,
National Academy of Sciences of Ukraine,
45 Nauki prospect, Kiev 03028, Ukraine

## Introduction

Self-assembled (In,Ga)As/GaAs quantum dots (QDs) demonstrate many favorable physical properties that makes them suitable for numerous device applications [1–4]. They possess high radiative efficiency and easily controllable areal densities; allow engineering of the energy levels permitting efficient carrier injection from a semiconductor matrix. Typically, (In,Ga)As/GaAs QDs have $\sim$2–5 nm height and $\sim$20–50 nm base width. Due to small QD sizes and high confinement potential, the electron and hole states are fully quantized and their wavefunctions are strictly localized within the QD area with a $\delta$-like density of states. Therefore, the self-assembled QDs can be treated to some extent as nearly ideal zero-dimensional (0D) systems behaving themselves like a "frozen ideal gas".

Each individual QD offers several advantages as a source for single photons. It has high oscillator strength and narrow spectral linewidth ($\sim$0.01 meV) and does not suffer from photobleaching or shelving. However, these idealizations have to be substantially modified in case of QD densities lying in the range of $\sim 10^{10}$–$10^{11}$ cm$^{-2}$. These densities result in mean dot separation of the order of tens to hundreds of nanometers which is comparable with the sizes of the individual QDs. Unavoidable size fluctuations within the QD ensemble lead to an additional inhomogeneous broadening of the optical spectra, frequently making the observation of the intrinsic 0D behavior difficult. Another characteristic of QD ensemble the interdot coupling is usually grouped into two categories with regard to whether it occurs via overlapping wave functions (electronic coupling) of the spatially separated QDs or via long-range electromagnetic interactions.

Depending on the strength of electronic coupling between neighboring QDs, their individual electronic states

and the relaxation of the photo-excited carriers through those states can be significantly altered. In the case of strong coupling, they can form QD molecules [5], resulting in new physics and a number of applications such as an excitonic qubit system with potential scalability [6]. In the case of intermediate or weak coupling, the energy and carrier transfer between QDs occurs through quantum–mechanical tunneling that substantially affects recombination, carrier injection, and lasing in the QD system [7–11].

The long-range radiative coupling between QDs in an ensemble can be interpreted in terms of successive emission and reabsorption of photons resulting in collective modes of several QDs. In this case, the exciton state of a single QD cannot be treated as a stationary state since its excitation in an individual QD will be transferred to other QDs [12]. In addition, energy transfer between dots can be in the form of an electrostatic dipole–dipole interaction, frequently cited as Förster energy transfer [13]. In the case of InP QDs with interdot distance of 7 nm, the Förster time for the excitation transfer between two QDs has been estimated [14] to be in the range of $10^2$–$10^3$ ps. This Förster transfer rate is proportional to the fourth power of the dipole moment matrix element and decays as the sixth power of the interdot distance [14]. Complementary to the Förster energy transfer, the polariton coupling is also expected to have a long spatial range, of the order of a few photon wavelengths. This mechanism results in the transfer of electron–hole excitation between distant QDs mediated by the emission and reabsorption of the transverse electromagnetic field [12]. Typical transfer rates attributed to polariton coupling are in the range of $10^{-3}$–$10^{-4}$ $ps^{-1}$. It is proportional to the square of the dipole moment matrix element and decays as the inverse of the interdot distance, if the transfer is mediated by a propagating field in two dimensions. Thus, in presence of radiative interaction, in fact, even very remote QDs cannot be considered as isolated systems, and the QD ensemble is expected to develop signatures of cooperative radiation or superradiation [15]. In order to strengthen the QD coupling through their radiation field, the use of semiconductor microcavities has been proposed and strong interaction between single QDs and the cavity mode has been already demonstrated [16].

In the case of QD ensembles with well-separated QDs, the fingerprint of cooperative effects in radiation is the change of the photoluminescence (PL) decay time with a change in the number of interacting QDs and their respective separation [12, 17]. The number and interdot separation of the dots can be varied using postprocessing of as-grown samples. For example, the dots could be covered by a mask containing small apertures through which the optical excitation as well as the collection of the signal is done. A lateral patterning of the sample surface offers another possibility. In this case, small mesa structures are fabricated which contain only a single QD or a few QDs. In case of CdSe/ZnSe QDs studied in Ref. [17], mesas of the same size were arranged in a grid-like pattern over an area larger than the size of the laser spot on the sample. Mesas of sizes down to a few tens of nanometers were etched into the QD sample removing the QDs from between the mesas. It has been shown [17] that the radiative interaction between QDs disappears with decreasing mesa size.

Recently, the new laterally ordered self-assembled (In,Ga)As/GaAs QD stack has been grown by molecular-beam epitaxy (MBE) [18]. QDs align in long rows forming QD chains. It has been found that the dot chains can be substantially increased in length by the introduction of growth interruptions during the initial stages of growth of the GaAs spacer layer. The growth procedure has been also used to create a template to arrange InAs dots into chains with a predictable dot density. The resulting dot chains offer the possibility to engineer interdot coupling for novel physical phenomena and potential devices. Here, the distance between neighboring QD chains can be made sufficiently large as to prevent the immediate electron–hole wavefunction tunneling as well as the Förster energy transfer between QDs belonging to different chains. This looks like as a natural mesa between chains. The objective of our research is the study of the peculiarities of interdot coupling in these new laterally ordered self-assembled (In,Ga)As/GaAs QD structures. In this case, we can expect the superradiance effect from the dot-chain ensemble. It is important that in-chain interdot coupling is easily changeable also thus permitting to study the cooperative effects caused by immediate interdot carrier tunneling.

We use the multilayer (In,Ga)As/GaAs dot-chain structure to reveal various cooperative effects arising both through overlapping wave functions of the spatially separated QDs and through long-range radiative interactions between QDs. "Experiment" includes the details of sample growth together with results of AFM analysis of the grown structure. The details of the PL are given. "Temperature cw PL measurements" includes the results of the temperature investigation of the cw PL. This results in information about the energy scheme of the system and provides evidence of interdot coupling and carrier transfer in QD chains. "Time-resolved PL measurements and mechanisms of interdot coupling" represents the results of the time-resolved PL measurements and contains the theoretical model used for the interpretations of the time-resolved PL data. Last section contains concluding remarks.

## Experiment

The multilayer (In,Ga)As/GaAs dot-chain structures were prepared in order to study the actual mechanisms of

interdot coupling which lead in part to the appearance of cooperative effects. $In_xGa_{1-x}As$ QDs were grown by molecular beam epitaxy (MBE) on semi-insulating GaAs (100) substrates such that dot chains form [18]. Following a 0.3-μm GaAs buffer layer grown at 580°C, the growth of $In_{0.4}Ga_{0.6}As$ QDs capped by 60 MLs of GaAs, both at 540°C, was repeated for a 15 layer superlattice. The $In_{0.4}Ga_{0.6}As$ QD layers were grown by the deposition of 8.5 ML of material. A final QD layer was grown and left uncapped for morphology analysis. The atomic force microscopy (AFM) image of the final, uncapped QD layer, Fig. 1a, demonstrates that these InGaAs QDs are formed in chains along the [0-11] direction. Figure 1b shows the Fourier transformed AFM image of an area with sizes $4 \times 4$ μm$^2$. The arrows pointed out the maxima along the directions of the QD alignment, [0-11] and [011]. Figure 1c presents a histogram of the QD aspect ratio. It is seen that the mean aspect ratio is ~0.11. Based on these results, the average spacing between chains is estimated to be 90 nm, while the separation between QDs in the chains is around 45 nm, close to the lateral size of QDs. As a result, it is expected that any observed lateral electronic coupling will be predominantly between the QDs in a single chain and negligible between interchain QDs. However, analysis of the PL reveals a much more complicated system of interaction and coupling between the dots. Note that in our multilayer structures the GaAs spacer between adjacent QD layers was thick enough (approximately 60 MLs thick) to prevent any vertical QD ordering. In this case, adjacent QD layers can be considered as independent QD systems (see e.g. Ref. [11]) and many layers serve predominantly to enhance the total PL gain.

The PL was performed using the 532-nm line from a frequency doubled Nd:YAG (neodymium-doped yttrium aluminum garnet) laser for continuous-wave PL excitation and the 2-ps pulses at $\lambda_{exc} = 750$ nm from a mode-locked Ti:sapphire laser for transient PL measurements. The optical pulse train at 76 MHz and an excitation density that was varied between $10^9$ and $2 \times 10^{14}$ photons/(pulse × cm$^2$) was used. The steady-state PL signal from the sample was dispersed by a 0.5-m single-grating monochromator and detected by a LN-cooled OMA V: InGaAs photodiode detector array. The PL transients were detected with a Hamamatsu synchroscan streak camera C5680 with an infrared enhanced S1 cathode. The overall time resolution of the system used in the time-resolved PL measurements was ~15 ps.

## Temperature cw PL Measurements

In order to get the information about both the energy scheme of the InGaAs/GaAs dot chain sample and the channels of the interdot carrier transfer, the temperature-dependent PL spectra are measured (Fig. 2). The low temperature ($T = 10$ K) and low excitation intensity ($I_{exc} = 0.4$ W/cm$^2$) cw PL measurements reveal a single peak for the ground state exciton emission with a maximum at $E_{max} = 1.247$ eV and full width at half maximum (FWHM) of $\Gamma \sim 48$ meV (Fig. 2). Increasing the temperature from 10 K up to 300 K shifts the PL band to the red by ~67 meV and broadens almost twice, up to ~87 meV. At the temperatures as high as 150 K, the PL is found to broaden asymmetrically, favoring the higher energy. The results of fit with two Gaussians, $E^1_{max} = 1.202$ eV, $\Gamma_1 = 49$ meV and $E^2_{max} = 1.238$ eV, $\Gamma_2 = 60$ meV, are

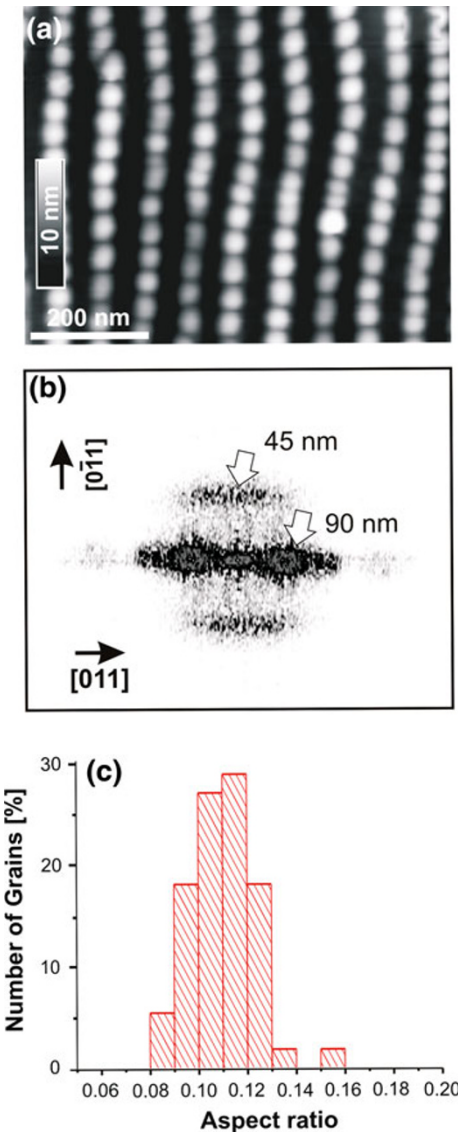


**Fig. 1** **a** AFM image of the uncapped (In,Ga)As/GaAs QD structure. **b** Fourier-transformed AFM image of an area with sizes $4 \times 4$ μm$^2$. The *arrows* pointed out the maxima along the directions of the QD alignment, [0-11] and [011]; **c** Histogram of QD distribution by the aspect ratio

shown in the PL spectrum measured for $T = 150$ K by dashed lines (Fig. 2). Therefore, the high temperature asymmetry is partly a result of thermal population of the higher energy confined states in the dots. More precise behavior of the PL peak maximum and the FWHM versus temperature is shown in Fig. 3. The temperature dependence of the FWHM (Fig. 3a) demonstrates a non-monotonic behavior. It reaches a minimum at ~80 K and then grows significantly with increasing temperature. The PL redshift (~32 meV, see Fig. 3b) is greater than the redshift of InAs (~13 meV, curve 3 in Fig. 3b) or GaAs (~17 meV, not shown here) upon increasing the temperature from 10 K to 100 K.

The initial PL spectrum narrowing in the temperature range between 10 and 80 K is ascribed to thermally induced carrier transfer between the QDs within each chain. According to a simple thermionic model [19, 20], at low $T$, carriers are "frozen" randomly into the QD states (after initial partial redistribution) due to the tunneling between QDs within each chain. With increasing $T$, carriers are expected to be thermally activated outside the dots into the 2D InGaAs wetting layer (WL) or GaAs barrier and/or hopping between dots will favor a drift of carriers toward the dots having lower ground state energies. This results in a narrowing of the PL spectrum and a redshift for the PL peak that is larger than expected from the thermal shrinkage of the InAs band gap under elevating $T$. In order to describe such a process, one can use either the rate equation model [19] or a simplified quasi-thermodynamic model [20] that introduces a temperature dependent function $\beta(T)$ allowing to parameterize the degree of thermalization of carriers. This function continuously interpolates between the well-defined low and high-temperature limits

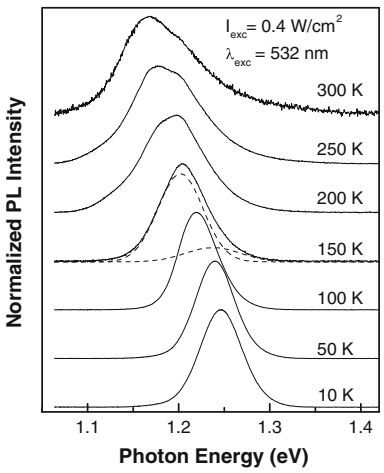


**Fig. 2** Normalized PL spectra for the multilayer $In_{0.4}Ga_{0.6}As/GaAs$ QD chain sample measured at different temperatures. For clarity, the spectra are vertically shifted with respect to each other. Two Gaussians best fitting the PL spectrum measured at $T = 150$ K are shown by *dashed lines*

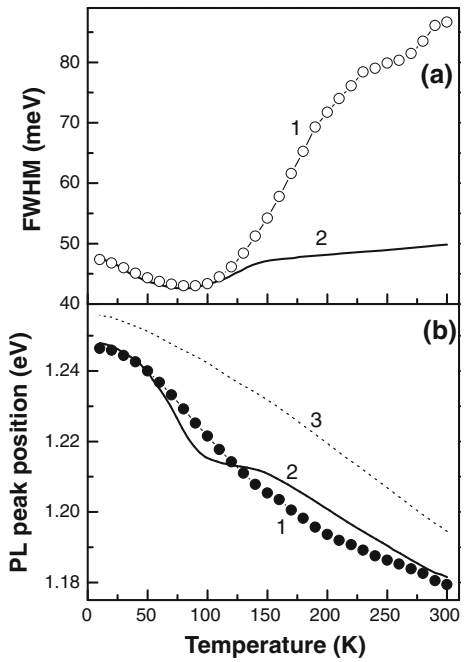


**Fig. 3** Temperature dependences of **a** FWHM (*curve 1*), and **b** PL band maximum $E_{max}$ (*curve 1*) measured in the QD sample. The results of fit with the set of parameters $\Delta = 15$ K and $T_{th} = 60$ K to Eqs. (1) and (2) are shown by *curve 2* in Fig. 3a, b. Temperature dependence of InAs energy gap followed the Varshni law [22] is given by *curve 3* in Fig. 3b

of the carrier distribution function and describes the observed peculiarities in the PL spectra with just two fitting parameters. In fact, such a description is equivalent to the assumption that partially thermalized carriers are still described by equilibrium statistics, but with a higher effective temperature $T_{th}$. Following to Ref. [20], the QD PL spectra ($I(E)$) can be treated using a relation like

$$I(E,\ T) = I_0(T) \times \exp\left\{-\frac{1}{o^2}\left[(A/(E-E_g))^2 - (A/(E_0-E_g))^2\right] + \beta(T)E/k_BT\right\} \quad (1)$$

with $I_0(T)$ being the temperature-dependent scale factor [21] and $E_g$ representing the temperature-dependent energy gap for InAs described, say, by the Varshni formula [22]. Parameter $A$ enters the relationship between the transition energies and the dot sizes [23] and is taken to be equal $A = 2.37$ eV nm$^{1/2}$ for our QDs. The QD ensemble is characterized by a Gaussian size distribution with a variance $o^2/2$ and mean basal length $a_0$ corresponding to the ground state transition energy $E_0$. The thermalization function $\beta(T)$ reflects all the carrier dynamics through the multiple pathways and can be approximated by expression [20]

$$\beta(T) = [1 + \exp\{-(T - T_{th})/\Delta\}]^{-1} \quad (2)$$

with $T_{\text{th}}$ and $\Delta$ being the only two fit parameters of the model. $T_{\text{th}}$ is the temperature when $\beta = 0.5$ and $\Delta$ corresponds to the temperature interval over which the transition from a "glassy" to a quasi-equilibrium state occurs.

Using Eqs (1) and (2) with the set of parameters $E_0 = 1.247$ eV and $\Delta = 48$ meV taken at the lowest temperature ($T = 10$ K) for a Gaussian describing the low temperature PL spectrum (Fig. 2), we find the best fit of the FWHM (T) (Fig. 3a) and $E_{\max}(T)$ (Fig. 3b) dependences with the parameters $\Delta = 15$ K and $T_{\text{th}} = 60$ K in the temperature range from 10 to 125 K. While the theoretical analysis carried out earlier is applied only for the ground state QD transitions our fit is valuable in the temperature range, where the contribution of the excited states is negligible. It follows from Fig. 2 that this range spreads from ~10 K up to ~150 K. It is important to note that the narrowing of PL the band width with an increase in temperature from ~10 to 100 K (see Fig. 3a) is not intuitive. One might expect the contrary, i.e., the FWHM increasing due to thermal broadening. Therefore, a good fit of the FWHM (T) dependence in this temperature range supports well the description of data in terms of the quasi-thermodynamic model presented earlier. In turn, the description of the $E_{\max}(T)$ dependence (see Fig. 3b) in the low-temperature range requires more elaborate analysis of the physical processes that determine the band-gap behavior in the QD system with increased temperature, e.g., electron–phonon coupling. The absence of such analysis can be in part an origin for the absence of a perfect fit for the $E_{\max}(T)$ data shown in Fig. 3b performed using the Varshni formula [22] for the temperature dependence of the energy gap in InAs QDs. For higher temperatures, the contribution of the excited states in the FWHM formation becomes significant leading to a significant deviation of calculated dependences from measured dependences observed in Fig. 3 in the temperature range above 150 K. Significantly small $T_{\text{th}}$ value in comparison with that $T_{\text{th}} = 127$ K found earlier for the InAs/GaAs QDs [19, 20] gives evidence of the existence of non-thermal relaxation mechanism favoring the thermalization of the QD system even at the lowest temperatures. Such a mechanism is the interdot tunneling caused by the electronic coupling between the dots of the same chain. In this case, carriers escape from the smaller QDs with higher ground state energy to the larger QDs with lower ground state energy. Such escape results in the higher population of the lower energy QD states in comparison with the population of the energy states of smaller QDs under the steady-state PL excitation and equal rate of the carrier trap on the small and large QDs. As a result, the PL band of the QD ensemble, which possesses a symmetric QD size distribution described by a Gaussian, has to be asymmetric with a more abrupt high-energy side. Introducing the asymmetry measure as the difference $\delta I = I(E_{\max} - |\delta|) - I(E_{\max} + \delta)$, $\delta = E - E_{\max}$, one can expect the positive asymmetry in case of low temperatures. Such determined asymmetry of the PL band is shown in Fig. 4. It occurs positive at the T = 10 K evidencing the non-thermal carrier distribution in the QD ensemble at low temperatures. Further temperature increase leads to the subsequent temperature population of the higher energy levels of smaller QDs thus decreasing the PL band asymmetry and finally switches the sign of asymmetry to the negative one. Such a behavior of the PL band asymmetry under the temperature increasing is demonstrated in Fig. 4. As one can see from Fig. 4, the well-pronounced PL band develops at the high-energy side of the dominant PL band. This band in the difference spectrum is shifted by ~38 meV from the PL peak position toward higher energy that quite well correlates with the energy difference $E^2_{\max} - E^1_{\max} = 38$ meV found from the PL line shape analysis carried out in Fig. 2 for $T = 150$ K. Our calculations of the QD energy spectrum show that in the $In_{0.4}Ga_{0.6}As/GaAs$ QD with the aspect ratio ~0.1 only one level $e_1$ is generated in the conduction band and at least two levels of heavy hole states ($hh_1$ and $hh_2$) arise in the valence band. Thus, we ascribe the main PL peak to the $e_1 \rightarrow hh_1$ intradot transition, whereas complementary high-energy peak arising at high temperatures is assigned to the $e_1 \rightarrow hh_2$ transition developing due to the thermal population of the $hh_2$ hole state. This additional transition significantly modifies the PL line shape at higher temperatures (Fig. 2) and introduces additional PL band broadening resulting in a significant deviation of the calculated temperature dependences from measured temperature dependences of FWHM and PL $E_{\max}$ within the temperature range 150–300 K (Fig. 3a, b). It is clear that the asymmetry of the PL band, measured directly (Fig. 4), gives information about both the intra- and interdot-chain carrier relaxation. Thus, it provides more information than one can obtain, say, from a Gaussian fit of the PL spectra (Fig. 2).

Analysis of the temperature dependence of the integrated PL for the multilayer $In_{0.4}Ga_{0.6}As/GaAs$ QD chain sample gives further verification of the contribution from the $e_1 \rightarrow hh_2$ QD transition. Figure 5 shows this dependence. At least three Arrhenius-type activation energies can be extracted from the plot in Fig. 5: $E^a_{2D} = 221$ meV, $E^a_{1D} = 144$ meV, and $E^a_h = 42$ meV. $E^a_h = 42$ meV quite satisfactorily agrees with the energy 38 meV extracted from the high temperature difference PL spectra (Fig. 4) for the $e_1 \rightarrow hh_2$ transition. The energy $E^a_{2D} = 221$ meV we ascribe to the transition from the QD electron ground state ($e_1$) to the 2D conduction band ($e^{WL}_1$) of WL, $e_1 \rightarrow e^{WL}_1$. Indeed this predicts the 2D WL in our system to be ~1.468 eV which is very close to the energy 1.445 eV

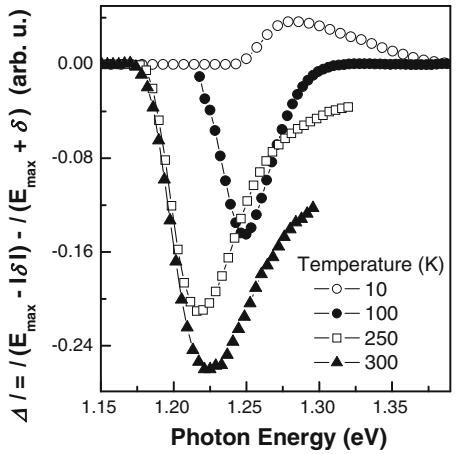


**Fig. 4** PL band asymmetry measured as difference $\delta I = I(E_{\max} - |\delta|) - I(E_{\max} + \delta)$, $\delta = E - E_{\max}$ for various temperatures. It is seen that low-temperature ($T = 10$ K) asymmetry is positive. The change of asymmetry sign evidences the appearance of the $e_1 - \mathrm{hh}_2$ QD transition and the predominant temperature population of the shallow QD states at high temperatures

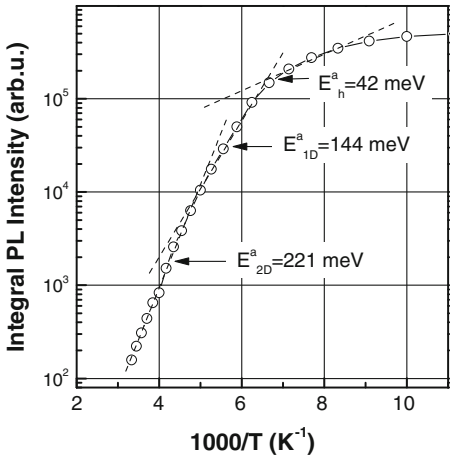


**Fig. 5** Semi-logarithmic plot of the integrated PL versus inverse temperature for the multilayer $In_{0.4}Ga_{0.6}As/GaAs$ QD chain sample. Three Arrhenius-type activation energies are extracted from the plot: $E^a_{2D} = 221$ eV, $E^a_{1D} = 144$ meV, and $E^a_h = 37$ meV

that has been observed for the 2D $In_{0.36}Ga_{0.64}As$ WL in similar QD samples under high optical pumping [24]. We were not able to saturate the QD states to see the WL in our samples due to the large density of dots. The energy $E^{\mathrm{a}}_{1\mathrm{D}} = 144$ meV we ascribe to the transition from the QD ground states to a 1D WL. Its energy is of about 1.391 eV. The existence of such WL is specific for the dot chain sample and has been proved recently by means of scanning electron, transmission electron, and atomic force microscopies [25] as well as by optical spectroscopy [26]. It has been shown that in addition to the conventional 2D WL involved in the Stranski–Krastanov growth a 1D-postwetting layer along the [01 − 1] direction arises that connects the QDs in each chain. Whereas the 2D WL exists before the QD chains form, the 1D-postwetting layer develops during the GaAs capping of already existing dot chains. It arises due to anisotropic surface diffusion of In atoms that accompanies the change in strain profile during capping and therefore produces the steady-state material distribution that includes a 1D-postwetting layer as a result.

Thus, the existence of various discrete and continuous states in the multilayer $In_{0.4}Ga_{0.6}As/GaAs$ QD chain sample substantially complicates the real picture of relaxation and coupling of the QDs. Based on the temperature dependence of the PL spectra, we can distinguish the low temperature effects caused by the in-chain interdot coupling and high temperature effects related to the QD coupling through the WL and GaAs barrier states. To go further, we focus on the low-temperature interdot coupling. We have demonstrated the cooperative effects caused by in-chain, interdot electronic coupling that becomes transformed into a change of the low temperature PL band and its line-shape. The features related to the interdot-chain, long-range radiative coupling are explored by means of time-resolved PL spectroscopy.

## Time-Resolved PL Measurements and Mechanisms of Interdot Coupling

The low temperature PL transients for the multilayer $In_{0.4}Ga_{0.6}As/GaAs(001)$ QD chain sample are shown in Fig. 6. The excitation density is chosen to be comparatively low in order to provide the mono-exponential PL decay following the law $I_{\mathrm{PL}}(t) = I_{\mathrm{PL}}(t_0)\exp\{-t/\tau_{\mathrm{d}}\}$ under excitation with different wavelengths. Here, the time $t_0$ corresponds to the beginning of declining part of the $I_{PL}(t)$ dependence and is set to be 0 in further analysis. The rate of decay is characterized with time $\tau_{\mathrm{d}}$. The characteristic rise time for all PL transients is found to not exceed ~20 ps indicating that the carriers are trapped quickly by all QDs. Figure 6a shows the transients measured with the excitation wavelength $\lambda_{\mathrm{exc}} = 750$ nm and the detection wavelengths $\lambda_{\mathrm{det}} = 930$ nm, 950 nm, 995 nm, and 1030 nm covering the region of the QD ground state emission. For comparison the laser pulse is also shown indicating that the observed PL decay is related to the QD system response only. Figure 6b shows the transients measured at the peak of the ground state emission, $\lambda_{\mathrm{det}} = 995$ nm, with pulsed laser excitation varied between $\lambda_{\mathrm{exc}} = 720$ nm (above the GaAs bandgap) and $\lambda_{\mathrm{exc}} = 870$ nm (below the GaAs bandgap and the InGaAs WL as shown in "Temperature cw PL measurements"). The observed exponential PL decay is well characterized by a single $\tau_{\mathrm{d}}$ value depending nevertheless both on the $\lambda_{\mathrm{exc}}$ and $\lambda_{\mathrm{det}}$. Figure 7 summarizes the $\tau_{\mathrm{d}}(E_{\mathrm{det}})$ data measured for

various excitation energies $E_{exc}$. The $\tau_d(\tilde{E}_{det})$ dependences are plotted versus the difference $\tilde{E}_{det} = E_{exc} - E_{det}$. Qualitative analysis of all $\tau_d(\tilde{E}_{det})$ dependences allows four items to be explained: i) rapid increasing of $\tau_d(\tilde{E}_{det})$ with decreasing $E_{det}$ throughout the QD PL spectrum; ii) reaching the maximal $\tau_d(\tilde{E}_{det})$ when $E_{det}$ reaches the PL maximum; iii) decreasing the maximal $\tau_d(\tilde{E}_{det})$ values with decreasing the excitation energy $E_{exc}$; and iv) appearance of the dip on the $\tau_d(\tilde{E}_{det})$ dependences for the detection energies lower than $E_0$. In order to address these four points we involve two different mechanisms of interdot coupling and the mechanisms of QD coupling with the host material and inherent defects finally affecting the $\tau_d$ value.

## Electronic Wave Function Interdot Coupling

Figure 8 shows $\tau_d(E_{det})$ dependences measured at $E_{exc} = 1.722$ eV and $E_{exc} = 1.477$ eV together with the normalized low temperature PL spectrum. We find these dependences resembling the typical $\tau_d(E_{det})$ dependences observed earlier in dense QD arrays [27, 28], which were described using lateral interdot transfer. Taking into account our finding of "Temperature cw PL measurements" concerning the in-chain interdot coupling, we first apply this description to our dot chain sample. The carrier dynamics in the QD system under excitation with a weak

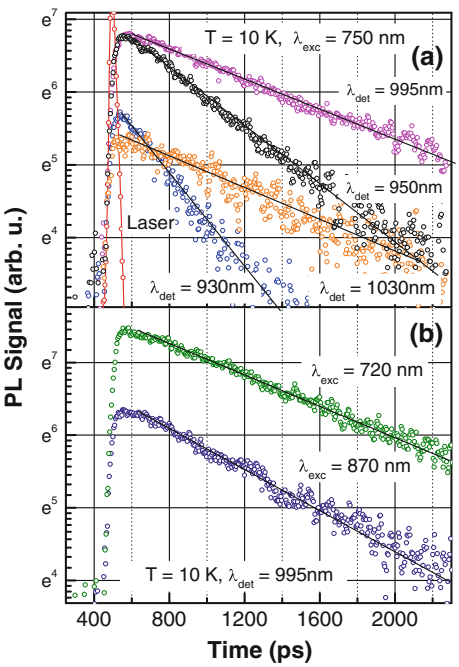


**Fig. 6** **a** Low-temperature PL transients measured at various $\lambda_{det}$ for a constant excitation wavelength $\lambda_{exc} = 750$ nm in the multilayer $In_{0.4}Ga_{0.6}As/GaAs$ QD chain sample. $\lambda_{det} = 995$ nm corresponds to the PL maximum. Laser pulse presents the response of the detecting system. **b** PL transients measured under two different $\lambda_{exc}$ at the position of the PL maximum, $\lambda_{det} = 995$ nm

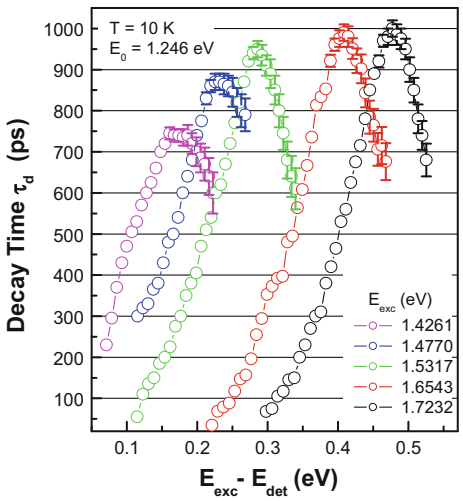


**Fig. 7** The $\tau_d(\tilde{E}_{det})$ data measured for various excitation energies $E_{exc}$. The $\tau_d(\tilde{E}_{det})$ dependences are plotted versus the difference $\tilde{E}_{det} = E_{exc} - E_{det}$. $E_0 = 1.246$ eV presents the position of the low temperature PL maximum

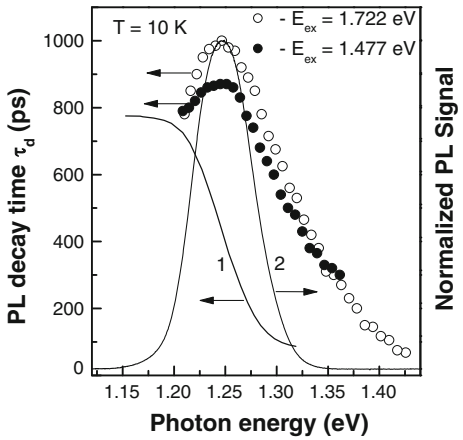


**Fig. 8** The $\tau_d(E_{det})$ data measured for two different excitation energies (*symbols*) and simulated $\tau_d(E_{det})$ dependence (*curve 1*) using the rate Eqs. (3), (5), and (6) with $\tau_{op} = 1$ and $\tau_T = 1.4$ ns (*solid line*). Normalized PL spectrum (*curve 2*) is given for $T = 10$ K

electromagnetic field can be treated with a system of rate equations. The lateral coupling is introduced through tunneling along the (In,Ga)As/GaAs QD chains as has been revealed recently [29]. In this case, the change of the population, $n = n(E)$, of the QD ground state $E$ for QD ensemble excited by the $E_{exc}$ photon is given by the equation [10]

$$\frac{dn(E,\ t)}{dt} = -\frac{n(E,t)}{\tau_{op}(E,E_{exc})} - R_1(E,t) + R_2(E,E_{exc},t). \quad (3)$$

Here, $1/\tau_{op}(E,\ E_{exc})$ represents the rate of the radiative recombination, $R_1(E,\ t)$ represents the rate at which the QD population decreases through tunneling processes, and $R_2(E,\ E_{exc},\ t)$ represents the QD capture rate from the

reservoir of photo-excited electrons. Taking into account that the PL intensity $I_{PL}(t) \propto n(t)$, one can introduce the PL decay time like a formula

$$\tau_d(E) = \left(\frac{d}{dt}\ln\left(\frac{n(0)}{n(E,t)}\right)\right)^{-1} \quad (4)$$

The explicit form of the relaxation terms introducing the tunneling time $\tau_T$ for the lateral carrier transfer is given by

$$R_1(E,t) = n(E,t)\int_0^E dE' D(E')[N(E') - n(E',t)]/\tau_T(E,E'), \quad (5)$$

$$R_2(E,E_{exc},t) = [N(E) - n(E,t)]\int_E^\infty dE' n(E',t)/\tau_T(E',E) + G(E,E_{exc})[N(E) - n(E,t)], \quad (6)$$

$$N(E) - n(E,t) \geq 0. \quad (7)$$

Here, $N(E)$ is the number of QDs with the ground state emission energy $E$; $D(E)$ is the density of states function; $\tau_T(E, E')$ is the tunneling time from the state $E$ to the state $E'$, and $G(E, E_{exc})$ is the carrier generation rate in the state $E$ by light with energy $E_{exc}$. For the QD ensemble, the $D(E)$ is taken as a Gaussian, $D(E) = \left(A\sigma^{-1}(\pi/2)^{-1/2}\right)\exp\left[-2(E-E_0)^2/\sigma^2\right]$ (see "Temperature cw PL measurements"). In fact Eq. (3) with the relaxation terms (5) and (6) describes carrier dynamics with a cascade-like carrier transfer from upper states to the lower QD states defined by the tunneling rate $\tau_T^{-1}(E,E')$. This equation allows for consideration of non-linear effects as well because the inequality (7) must hold strictly.

For the sake of simplicity, we define a single tunneling time for all QDs, $\tau_T(E, E') = \tau_T$, and independent of $E$ and $E_{exc}$ set the optical recombination time as $\tau_{op}(E, E_{exc}) = \tau_{op} = 1$ ns. Then, considering the case of a weak electromagnetic field and comparatively slow interdot transfer, $\tau_T = 1.4$ ns [10, 27, 28], we also assume that $N(E) >> n(E, t)$. This allows us to linearize Eqs. (3), (5), and (6) and solve them numerically. The result of such simulation is shown in Fig. 8 by solid line. This demonstrates that the mechanism of interdot carrier tunneling allows us to qualitatively reproduce the observed rise of $\tau_d(E_{det})$ with decreasing $E_{det}$ through the range of the QD PL spectrum. The difference between experimental and calculated dependences can be reduced significantly if the saturation of the QD ground states is taken into account. This would allow us to shift the energies at which the calculated $\tau_d(\lambda_{det})$ function saturates closer to the PL maximum as it is observed for the measured $\tau_d(\lambda_{det})$ dependence. Thus, this mechanism of in-chain interdot tunneling is consistent with two items mentioned earlier: rapid increasing the $\tau_d(E_{det})$ value within the QD PL spectrum and reaching the maximal $\tau_d(E_{det})$ values at the energy corresponding to the energy of PL maximum. However, this simplified model cannot reproduce in principle two experimental facts: decreasing the maximal $\tau_d(E_{det})$ values with decreasing the excitation energy $E_{exc}$ and appearance of the dip on the $\tau_d(E_{det})$ dependences for the detection energies lower than $E_0$. These two features are formed by complementary mechanisms: interdot coupling through radiation field and QD coupling with the host materials and inherent defects.

## Radiation Field Interdot Coupling

In analyzing the $\tau_d(E_{det})$ dependence in terms of Eqs. (3), (5) and (6), we assumed that $\tau_{op}(E, E_{exc}) = \tau_{op} = \text{const}$. However, it has been shown [30–32] that $\tau_{op}$ depends on $E$ in QD systems and can be written as

$$\tau_{op}^{-1} \propto E\left\langle c\middle|e\circ\hat{P}\middle|v\right\rangle^2 \quad (8)$$

with $E$ being the emitted photon energy and $\left\langle c\middle|e\circ\hat{P}\middle|v\right\rangle$ being the optical matrix element for the conduction-valence band transition. According to Eq. (8), the $\tau_{op}$ value inversely depends on the emission energy ($\tau_{op}(E) \propto 1/E$). This monotonic behavior of $\tau_{op}$ can explain neither the dependence of $\tau_d$ on the $E_{exc}$ nor the saturation of $\tau_d$ function observed experimentally. Because the strongest change of $\tau_d$ takes place near the QD PL maximum, which is related to the emission of the most numerous QDs, we might attribute the change to a cooperative effect. The cooperative emission from optically coupled oscillators [12] has been revealed recently in a single layer of self-assembled CdSe/ZnSe QDs [17] and in the (In,Ga)As/GaAs dot-chain superlattices [33]. With optical collective interaction, the conventional radiation of $N$ identical oscillators transforms into two different radiant modes: a superradiant mode with a shorter lifetime $\tau_{spr} \approx \tau_{op}/N$ and a subradiant mode with lifetime $\tau_{sbr} \gg \tau_{op}$. Thus, the effective radiation rate is given by

$$\tau_{eff}^{-1} = \tau_{op}^{-1} + \tau_{spr}^{-1} + \tau_{sbr}^{-1} \cong \tau_{op}^{-1} + \tau_{spr}^{-1}. \quad (9)$$

Since $\tau_{sbr} \gg \tau_{op} > \tau_{spr}$, only the superradiant modes contribute significantly along with the radiative recombination time to the effective decay time. In our case, this description has to be extended to the cooperative emission of a certain number, $\Delta N(E)$, of optical modes corresponding to QDs emitting light with the same frequency. Then, the optical decay time will be given by

$$\tau_{eff}(E) = \tau_{op}(E)/[\Delta N(E) + 1]. \quad (10)$$

In a simplified description of continuous distribution of optical modes by energy, their density can be considered as

a Lorenzian. Thus, the number of modes within a range $\Delta E$ will be

$$\Delta N(E) = 2n_T \Delta E \frac{1}{\pi} \times \frac{\Gamma_{\text{op}}}{(E - E_0)^2 + \Gamma_{\text{op}}^2}, \tag{11}$$

where 2 stands for the double degeneracy of each QD ground state, and $n_T$ is the total number of dots. The dispersion width of optical modes, $\Gamma_{\text{op}}$, can be calculated by considering a total number of the excited optical modes, $N_T$, that depends on the excitation energy, $E_{\text{exc}}$, through

$$\frac{N_T}{n_T} = \frac{2}{\pi} \int_{-\infty}^{\infty} dE \frac{\Gamma_{\text{op}}}{(E - E_0)^2 + \Gamma_{\text{op}}^2} \tag{12}$$

This yield

$$\Gamma_{\text{op}} = \Delta E_{\text{w}}^0 \tan\left[\frac{\pi}{2}\left(\frac{N_T}{n_T} - 1\right)\right], \tag{13}$$

where $\Delta E_{\text{w}}^0 = E_{\text{exc}} - E_0$.

The important parameter characterizing the collective emission is the decay time at the PL maximum energy, $\tau_{\text{eff}}(E_0)$. According to Eqs. (10, 11), this parameter is reduced to

$$\tau_{\text{eff}}(E_0) = \tau_{\text{op}}(E_0)(\alpha/\Gamma_{\text{op}} + 1)^{-1} \tag{14}$$

It can be immediately compared with the measured data. Taking $\tau_{\text{op}}(E)$ in the form $\tau_{\text{op}}(E) = C_1/E$ as in Eq. (8), we fit Eq. (14) to the measured $\tau_{\text{d}}(E_0)$ with the set of parameters: $C_1 = 1.3$ ns $\times$ eV, $\alpha = 0.025$ eV, and $N_T/n_T = 1.113$. The result of best fit is shown in Fig. 9 by solid line together with measured $\tau_{\text{d}}(E_0)$ (open circles). The quantitative agreement of the $\tau_{\text{d}}(\tilde{E}_0)$ growth with the difference $\tilde{E}_0 = E_{\text{exc}} - E_0$ increasing between the theory and experiment gives strong support of the cooperative nature of the QD emission near the PL maximum.

Further evidence of the superradiance effect in our QD system arises from comparison of the $\tau_{\text{d}}(\lambda_{\text{det}})$ dependence under excitation both with $\lambda$ close to the PL maximum (quasi-resonant case) and far from the PL maximum (non-resonant case). It has been shown [17] that for the non-resonant condition $\tau_{\text{d}}(\lambda_{\text{det}})$ is mainly a result of the optical emission lifetime $\tau_{\text{op}}$, whereas for the quasi-resonant condition it equals $\tau_{\text{eff}}$. From Fig. 7, the $\tau_{\text{d}}(\lambda_{\text{det}})$ dependences can be seen to be different under non-resonant (*nr*) excitation condition and quasi-resonant (*qr*) conditions. Figure 10a displays the relative change in decay rate given by taking the ratio of the PL decay times under quasi-resonant excitation ($\lambda_{\text{exc}} = 870$ nm) and non-resonant ($\lambda_{\text{exc}} = 720$ nm) excitation. The ratio $\tau_{870}/\tau_{720}$ reveals the strongest change just in the vicinity of the maximum of the PL spectrum. Such a behavior of the $\tau_{870}/\tau_{720}$ ratio [33] serves as a fingerprint of the cooperative QD emission. Indeed, the continuous wave PL spectrum represents the

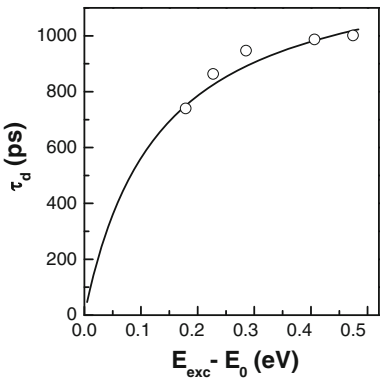


**Fig. 9** The measured (*open circles*) and calculated data from Eq. (14) with the set of parameters: $C_1 = 1.3$ ns $\times$ eV, $\alpha = 0.025$ eV, and $N_T/n_T = 1.113$ (*solid line*) $\tau_d(\tilde{E}_0)$ dependences versus the difference $\tilde{E}_0 = E_{\text{exc}} - E_0$

distribution of the ground-state energies of excitons in the QD ensemble which is in turn due to the QD size distribution. While the QD density is the highest in the center of the QD size distribution, the radiation field of the QDs is the strongest at a specific exciton ground-state energy corresponding to the maximum of the PL signal. Consequently, a radiative interaction has to be strongest between the QDs belonging to the central part of the QD size distribution, thus the change in radiation rate has to be strongest in the PL spectral maximum. This is what is observed experimentally in our QD sample. It is also shown in Ref. [10] that the change of the radiation rate ($\Delta = \tau_{\text{d,coupl}}^{-1} - \tau_{\text{d, uncoupl}}^{-1}$) caused by a radiative coupling between QDs has to be properly scaled because it depends linearly on the number of QDs, $N(\lambda)$, emitting with the wavelength $\lambda$, and decreases inversely with the distance between QDs, $R(\lambda)$. This leads to the change in the radiation rate as $\Delta(N(\lambda), R(\lambda)) \propto I^{3/2}(\lambda)$. We compared this dependence with the measured change in the PL decay time (Fig. 10b) presented in the form $\Delta\left(\tau_{\text{qr}}^{-1}(\lambda), \tau_{\text{nr}}^{-1}(\lambda)\right) = \tau_{\text{nr}}(\lambda)\tau_{\text{qr}}^{-1}(\lambda) - 1$ and found a good correlation, which indicates radiative coupling between QDs. We assume that this radiative coupling is dominant for the QDs belonging to different chains, whereas immediate electronic coupling dominates between the in-chain dots.

Independently, the superradiance contribution to the radiation rate in our system is revealed from the analysis of the $\tau_{\text{d}}(\lambda_{\text{det}})$ dependence measured at the PL band maximum for various excitation intensities. It is expected [33] that the $\tau_{\text{d}}(\lambda_{\text{det}})$ value must depend non-monotonicly on $I_{\text{exc}}$. Indeed, for the case of extremely low excitation intensity only a very small number of QDs are optically excited, and therefore the radiative cooperative effects should be negligible. Under increased excitation density, the superradiance mode becomes more significant, coupling the QDs of the ensemble and leading to a decrease of the $\tau_{\text{d}}(\lambda_{\text{det}})$ value.

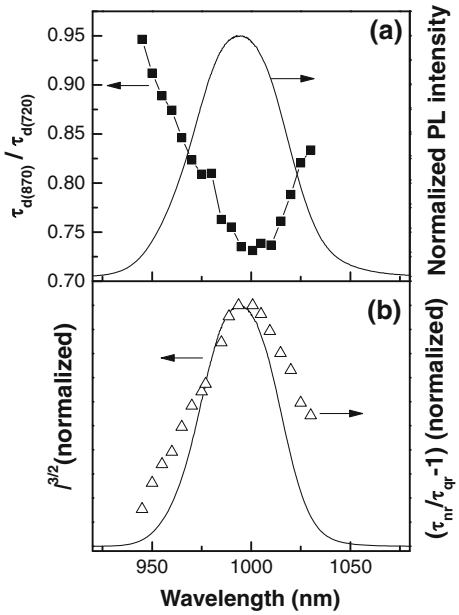


**Fig. 10** **a** The ratio $\tau_{870}/\tau_{720}$ (*symbols*) of the $\tau_d(\lambda_{det})$ measured under quasi-resonant ($\lambda_{exc} = 870$ nm) and non-resonant ($\lambda_{exc} = 720$ nm) excitations. The strongest change is seen just in the vicinity of the maximum of the normalized PL spectrum (*solid line*). **b** Normalized $\Delta\left(\tau_{qr}^{-1}(\lambda), \tau_{nr}^{-1}(\lambda)\right) = \tau_{nr}(\lambda)\tau_{qr}^{-1}(\lambda) - 1$ dependence (*symbols*) and normalized $I^{3/2}(\lambda)$ spectrum (*solid line*). Such a behavior of the measured $\tau_d(\lambda_{det})$ under non-resonant and quasi-resonant conditions evidences the cooperative radiative QD coupling

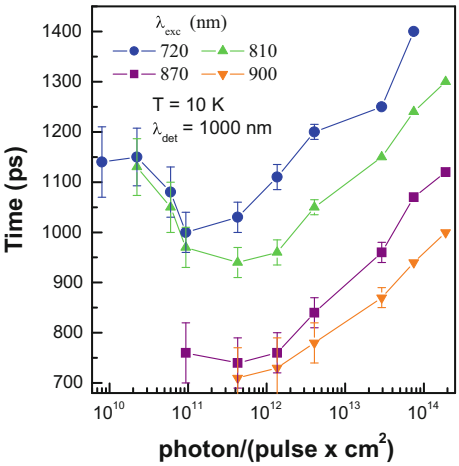


**Fig. 11** The $\tau_d$ dependence measured at the QD PL maximum in $In_{0.4}Ga_{0.6}As/GaAs$ QD chain sample versus excitation density for different excitation wavelengths. *Vertical bars* show experimental accuracy

Such a result is shown in Fig. 11 for the $In_{0.4}Ga_{0.6}As/GaAs$ QD chain sample. Here, the dependence of $\tau_d$ measured at the QD PL maximum on the excitation density is clearly demonstrated for various excitation wavelengths. One can see that at the lowest excitation densities ($\sim 10^{10}$ photons/(pulse $\times$ cm$^2$)) the $\tau_d$ value is practically invariable due to the absence of interdot radiative coupling. However, let us note that the experimental accuracy of the $\tau_d$ determination is rather low due to the noisy PL signal in case of lowest excitation densities. As a result, for $\lambda_{exc} = 870$ nm and $\lambda_{exc} = 900$ nm (see Fig. 11), we cannot reliably investigate the region of the lowest excitation densities. If the excitation intensity is raised the superradiance mode turns on strongly, coupling the QDs within the ensemble. Such a coupling tends to reduce the $\tau_d$ value, which is seen in Fig. 11 for the excitation wavelengths $\lambda_{exc} = 720$ nm and $\lambda_{exc} = 810$ nm. Further increase in the excitation density leads to a saturation of the QD ground states resulting in a progressive increase in the $\tau_d$ value. The appearance of a dip in the $\tau_d$ dependence on the excitation density in the range of very low excitation densities serves as a specific fingerprint of superradiance in our QD samples.

The appearance of the dip on the $\tau_d(\tilde{E}_{det})$ dependences for the detection energies lower than $E_0$ (see Fig. 7) can be attributed to the coupling of longitudinal optical phonons with confined electrons and holes in QDs and to the presence of deep levels allowing the holes tunnel to these states even at low temperatures [34]. The states of deep levels are closer to the states of larger QDs. Therefore, the hole tunneling is more effective for larger QDs that form the low energy side of the PL spectrum thus reducing the $\tau_d(\tilde{E}_{det})$ value observed experimentally in the spectral range below the QD PL maximum.

## Conclusions

Finally, peculiar dependences of the PL decay time on the excitation and detection energies are revealed in the multilayer $In_{0.4}Ga_{0.6}As/GaAs$ QD chain sample and ascribed to the peculiarities of the carrier and energy relaxation caused by both immediate electronic interdot coupling and long-range coupling through the radiation field. Summarizing, we have established: i) appearance of low temperature asymmetry of the PL band caused by the non-thermal carrier distribution through in-chain interdot wave function coupling. The energy scheme of the $In_{0.4}Ga_{0.6}As/GaAs$ QD chain sample is specified and 1D WL, 2D InGaAs WL, and the heavy hole excited states are identified from the temperature cw PL measurements: ii) the in-chain interdot carrier transfer forms the swing of the decay time $\tau_d$ versus detection energy dependence and can lead to the state saturation effect shifting the maximal $\tau_d$ value close to QD PL maximum; iii) superradiant mode of the emission field couples the QDs of different dot chains and leads to a significant change of the decay time value just in the vicinity of the QD PL maximum. This radiant interdot coupling defines the dependence of the $\tau_d$ value on the excitation wavelength. Coexistence of various mechanisms

of interdot coupling is determined here by special design of the QD samples providing effective interdot in-chain electronic coupling and effective radiative interchain coupling due to superradiance. This latter type of coupling could play a significant role in ultrafast applications.

**Acknowledgments** The authors acknowledge the financial support of the National Science Foundation of the U.S. through Grant # DMR-0520550.



## References

1. D. Bimberg, M. Grundman, N.N. Ledentsov, *Quantum dot heterostructures* (Wiley, New York, 1999)
2. M. Bayer, G. Ortner, O. Stern, A. Kuther, A.A. Gorbunov, A. Forchel, P. Hawrylak, S. Fafard, K. Hinzer, T.L. Reinecke, S.N. Walck, J.P. Reithmaier, F. Klopf, F. Schäfer, Phys. Rev. B **65**, 195315 (2002)
3. P. Michler (ed.), Single quantum dots: fundamentals, applications, and new concepts. Topics in Applied Physics, vol 90. (Springer, Berlin) 2003
4. D.J. Mowbray, M.S. Skolnick, J. Phys. D **38**, 2059 (2005)
5. M. Bayer, P. Hawrylak, K. Hinzer, S. Fafard, M. Korkusinski, Z.R. Wasilewski, O. Stern, A. Forchel, Science **291**, 451 (2001)
6. E. Biolatti, R.C. Iotti, P. Zanardi, F. Rossi, Phys. Rev. Lett. **85**, 5647 (2000)
7. R. Leon, S. Marcinkevicius, X.Z. Liao, J. Zou, D.J.H. Cockayne, S. Fafard, Phys. Rev. B **60**, 8517 (1999)
8. M. Paillard, X. Marie, E. Vanelle, T. Amand, V.K. Kalevich, A.R. Kovsh, A.E. Zhukov, V.M. Ustinov, Appl. Phys. Lett. **76**, 76 (2000)
9. G.G. Tarasov, Yu.I. Mazur, Z.Ya. Zhuchenko, A. Maaßdorf, D. Nickel, J.W. Tomm, H. Kissel, C. Walther, W.T. Masselink, J Appl. Phys. **88**, 7162 (2000)
10. J.W. Tomm, T. Elsaesser, Yu.I. Mazur, H. Kissel, G.G. Tarasov, Z.Ya. Zhuchenko, W.T. Masselink, Phys. Rev. B **67**, 045326 (2003)
11. I.Yu. Mazur, G.G. Tarasov, G.I. Salamo, Self-assembled quantum dots, in *Carrier transfer in the arrays of coupled quantum dots*, ed. by M.Zh. Wang (Springer, New York, 2008)
12. G. Parascandolo, V. Savona, Phys. Rev. B **71**, 045335 (2005)
13. Th. Förster, Ann. Phys. (Leipzig) **2**, 55 (1948)
14. A.O. Govorov, Phys. Rev. B **68**, 075315 (2003)
15. R. Jodoin, I. Mandel, Phys. Rev. A **9**, 873 (1973)
16. J.P. Reithmaier, G. Sek, A. Löffler, C. Hofmann, S. Kuhn, S. Reitzenstein, L.V. Keldysh, V.D. Kulakovskii, T.L. Reinecke, A. Forchel, Nature **11**, 432 (2004)
17. M. Scheibner, T. Schmidt, L. Worschech, A. Forchel, G. Bacher, T. Passow, D. Hommel, Nat. Phys. **3**, 106 (2007)
18. Z.M. Wang, K. Holmes, Yu.I. Mazur, G.J. Salamo, Appl. Phys. Lett. **84**, 1931 (2004)
19. S. Sanguinetti, M. Henini, M. Grassi Alessi, M. Capizzi, P. Frigeri, S. Franchi, Phys. Rev. B **60**, 8276 (1999)
20. B. Bansal, J. Appl. Phys. **100**, 093107 (2006)
21. E.C. Le Ru, J. Fack, R. Murray, Phys. Rev. **67**, 245318 (2003)
22. I. Vurgaftman, J.R. Meyer, L.R. Ram-Mohan, J. Appl. Phys. **89**, 5815 (2001)
23. M. Grundmann, O. Stier, D. Bimberg, Phys. Rev. B **52**, 11969 (1995)
24. Yu.I. Mazur, W.Q. Ma, X. Wang, Z.M. Wang, G.J. Salamo, M. Xiao, T.D. Mishima, M.B. Johnson, Appl. Phys. Lett. **83**, 987 (2003)
25. X. Wang, Z.M. Wang, B. Liang, G.J. Salamo, C.K. Shih, Nano Lett. **6**, 1847 (2006)
26. Z.M. Wang, Yu.I. Mazur, J.L. Shultz, G.J. Salamo, T.D. Mishima, M.B. Johnson, J Appl. Phys. **99**, 033705 (2006)
27. Yu.I. Mazur, J.W. Tomm, V. Petrov, G.G. Tarasov, H. Kissel, C. Walther, Z.Ya. Zhuchenko, W.T. Masselink, Appl. Phys. Lett. **78**, 3214 (2001)
28. Yu.I. Mazur, J.W. Tomm, G.G. Tarasov, H. Kissel, C. Walther, Z.Ya. Zhuchenko, W.T. Masselink, Physica E **13**, 255 (2002)
29. B.R. Wang, B.Q. Sun, Y. Ji, X.M. Dou, Z.Y. Xu, Zh.M. Wang, G.J. Salamo, Appl. Phys. Lett. **93**, 011107 (2008)
30. S. Malik, E.C. Le Ru, D. Childs, R. Murray, Phys. Rev. B **63**, 155313 (2001)
31. U. Bockelmann, Phys. Rev. B **48**, 17637 (1993)
32. M. Sugawara, Phys. Rev. B **51**, 10743 (1995)
33. Yu.I. Mazur, V.G. Dorogan, E. Marega Jr, G.G. Tarasov, D.F. Cesar, V. Lopez-Richard, G.E. Marques, G.J. Salamo, Appl. Phys. Lett. **94**, 123112 (2009)
34. Yu.I. Mazur, Zh.M. Wang, H. Kissel, Z.Ya. Zhuchenko, P.M. Lisitsa, G.G. Tarasov, G.J. Salamo, Semicond. Sci. Technol. **22**, 86 (2007)